

Mixed Layer Lateral Eddy Fluxes Mediated by Air–Sea Interaction

EMILY SHUCKBURGH

British Antarctic Survey, Cambridge, United Kingdom

GUILLAUME MAZE

Laboratoire de Physique des Océans, IFREMER, Plouzané, France

DAVID FERREIRA, JOHN MARSHALL, HELEN JONES, AND CHRIS HILL

Department of Earth, Atmospheric and Planetary Sciences, Massachusetts Institute of Technology, Cambridge, Massachusetts

(Manuscript received 11 January 2010, in final form 27 August 2010)

ABSTRACT

The modulation of air–sea heat fluxes by geostrophic eddies due to the stirring of temperature at the sea surface is discussed and quantified. It is argued that the damping of eddy temperature variance by such air–sea fluxes enhances the dissipation of surface temperature fields. Depending on the time scale of damping relative to that of the eddying motions, surface eddy diffusivities can be significantly enhanced over interior values. The issues are explored and quantified in a controlled setting by driving a tracer field, a proxy for sea surface temperature, with surface altimetric observations in the Antarctic Circumpolar Current (ACC) of the Southern Ocean. A new, tracer-based diagnostic of eddy diffusivity is introduced, which is related to the Nakamura effective diffusivity. Using this, the mixed layer lateral eddy diffusivities associated with (i) eddy stirring and small-scale mixing and (ii) surface damping by air–sea interaction is quantified. In the ACC, a diffusivity associated with surface damping of a comparable magnitude to that associated with eddy stirring ($\sim 500 \text{ m}^2 \text{ s}^{-1}$) is found. In frontal regions prevalent in the ACC, an augmentation of surface lateral eddy diffusivities of this magnitude is equivalent to an air–sea flux of 100 W m^{-2} acting over a mixed layer depth of 100 m, a very significant effect. Finally, the implications for other tracer fields such as salinity, dissolved gases, and chlorophyll are discussed. Different tracers are found to have surface eddy diffusivities that differ significantly in magnitude.

1. Introduction

Interactions at the ocean surface form an integral part of the variability of the earth system and in particular its climate. These interactions include thermodynamically mediated changes to the ocean heat budget; changes to the ocean salinity budget via evaporation and precipitation; exchanges of gases such as oxygen, carbon dioxide, and nitrous oxide; and processes influencing biological productivity. Ocean mesoscale eddies may modulate such interactions, particularly in eddy-rich regions such as the Gulf Stream, Kuroshio, and Antarctic

Circumpolar Current (ACC; Tandon and Garrett 1996; Greatbatch et al. 2007). In this paper, we will focus on the role that eddies play in determining the distribution of sea surface temperature (SST). Our results also have implications for the distribution of other surface tracer fields such as salinity and chlorophyll. Eddies contribute to the budgets of such fields through their role in lateral transport. This transport, however, is intimately connected to irreversible processes such as lateral small-scale mixing and damping processes associated with air–sea fluxes (Zhai and Greatbatch 2006a,b; Greatbatch et al. 2007). It is a quantification of the latter process that is the focus of attention here.

Figure 1 shows a wintertime instantaneous (Fig. 1a) and monthly-mean (Fig. 1b) net air–sea heat flux obtained from a global $1/8^\circ$ eddy-resolving model driven by observed atmospheric fields through bulk formulas that

Corresponding author address: Emily Shuckburgh, British Antarctic Survey, High Cross, Madingley Rd., Cambridge CB4 3BE, United Kingdom.
E-mail: emsh@bas.ac.uk

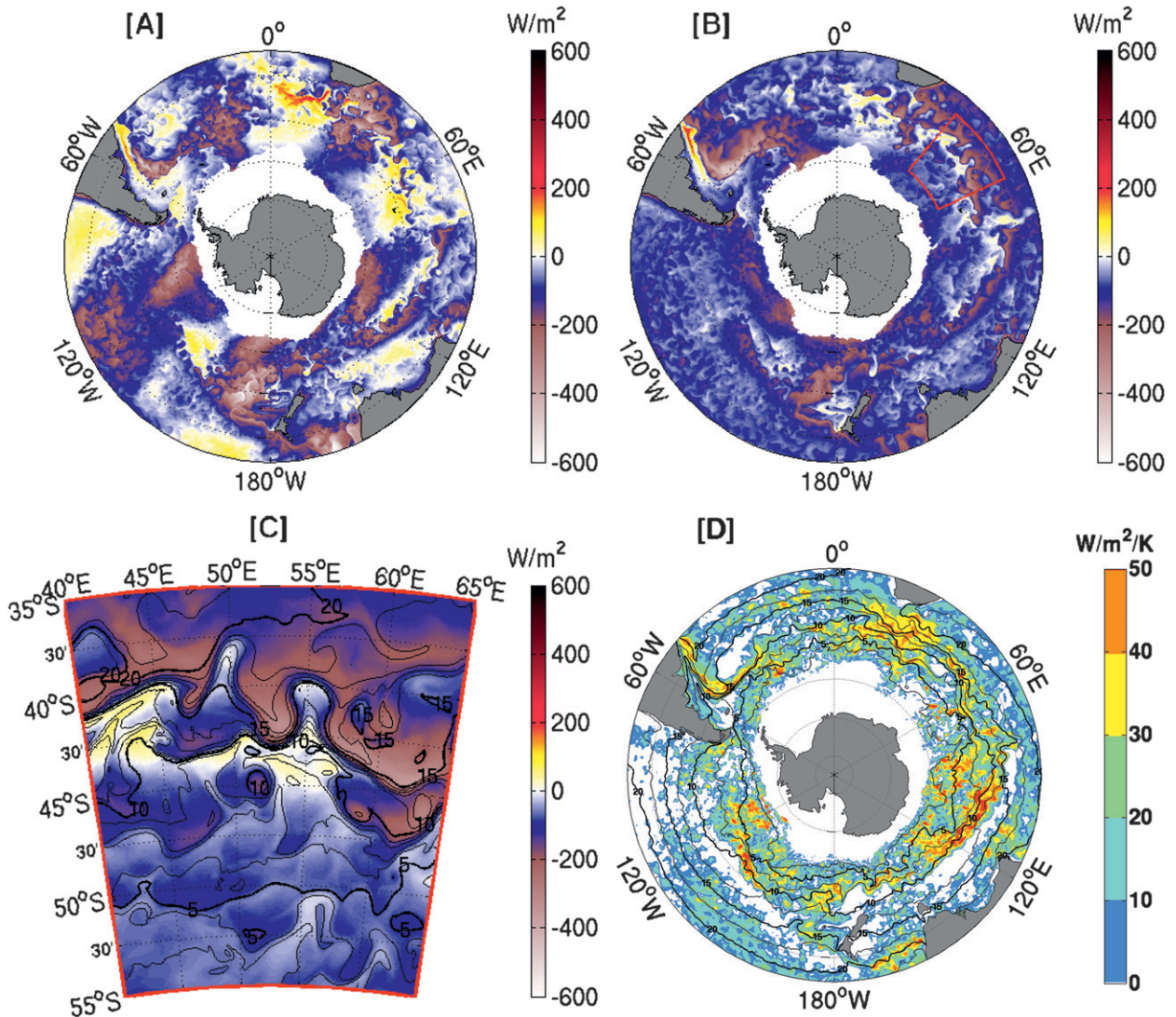


FIG. 1. (a) Daily mean of the sea surface heat flux Q for 5 May 2003 of the $1/8^\circ$ ECCO2 simulation. (b) Monthly mean of Q for May 2003. (c) A local zoom of (b), in the eddy-rich region around 60°E along the ACC and indicated by the red box in (b). Superimposed are SST contours for the same period (black thin: every 1°C; thick: every 5°C). (d) May 2002–April 2005 mean of $\alpha = -\overline{Q'T'}/T'^2$ with mean SST over the same period (thin black: every 2.5°C; thick black: every 5°C).

allow the evolving SST to modulate air–sea fluxes (see appendix for details). Only the eddy-rich Southern Ocean is depicted. The instantaneous field reveals two scales: one associated with the prevailing atmospheric synoptic-scale systems (~ 1000 km) and the other controlled by the ocean’s mesoscale variability (~ 20 km). The monthly-mean air–sea flux averages out the rapid synoptic-scale variability imposed by the atmosphere to reveal the smaller spatial-scale and longer time-scale modulation of air–sea fluxes by the ocean mesoscale. This modulation is very clear in the local zoom of monthly-mean patterns shown in Fig. 1c. The imprint of the ocean eddies is large, resulting in anomalous fluxes that often exceed $\pm 100 W m^{-2}$.

The modulation of air–sea fluxes on the eddy scale acts to damp eddies, as can be seen in Fig. 1d, which plots the damping rate $\alpha = -\overline{Q'T'}/T'^2$. Here, $\overline{Q'T'}$ is the eddy covariance of sea surface temperature T with the sea surface heat flux Q [see Eq. (9)]. We see that model eddies are damped in the Southern Ocean at a rate on the order of $\alpha = 20\text{--}40 W m^{-2} K^{-1}$.

Although the model results presented in Fig. 1 are used here only to illustrate the physics at play, it is worth briefly examining their relevance. The model might exaggerate the heat flux damping because it does not employ an atmospheric boundary layer scheme. Indeed, in the real world, air temperature would adjust to the SST anomalies, hence reducing the air–sea temperature

contrast and anomalous fluxes (for a simple model to rationalize the “reduced heat flux” damping due to the air–sea adjustment, see Barsugli and Battisti 1998). Using the Comprehensive Ocean–Atmosphere Data Set (COADS), Frankignoul et al. (1998) estimate that the surface air temperature adjustment reduces the heat damping by about a factor of 2, from 50 to 20 $\text{W m}^{-2} \text{K}^{-1}$. The value $\alpha = 20 \text{ W m}^2 \text{K}^{-1}$ is probably a lower bound for the real damping rate because the calculation was performed “locally” on each $5^\circ \times 5^\circ$ (latitude \times longitude) grid box of the dataset, not at the mesoscale, and the heat flux damping is likely to increase with decreasing spatial scales (Bretherton 1982; Zhai and Greatbatch 2006a). The Frankignoul et al. (1998) maximum estimate of $\alpha = 50 \text{ W m}^{-2} \text{K}^{-1}$ (no air temperature adjustment) provides an upper bound on this. The model damping rates we find here are consistent with those broad ranges. More importantly, although the exact rate is somewhat uncertain, it is the very fact that mesoscale SST anomalies are damped by air–sea heat fluxes, which is key here. This is a robust feature that does not depend on the details of the heat flux scheme in the model and is supported by observations (Bourras et al. 2004).

These results corroborate a standard assumption made in models (see Haney 1971) and also adopted here, in which an advected tracer representing SST is damped by a simple restoring boundary condition with a relaxation time scale λ^{-1} (where $\lambda = \alpha/\rho_0 C_p H$: ρ_0 is a reference ocean density, C_p is the specific heat of seawater, and H is the mixed layer depth). Moreover, patterns that form in this type of modeled SST-like tracer from the combined influence of stirring by mesoscale eddies and damping–dissipative effects are consistent with those found in SST from satellite observations (Abraham and Bowen 2002). Comparison of the spatial patterns in model and observational data from the southwest Tasman Sea has indicated a relaxation time scale of 20 days (Abraham and Bowen 2002). Simple bulk estimates suggest a time scale on the order of a few months (Bracco et al. 2009), and studies based on direct analysis of limited ship- and satellite-derived heat flux data for the Southern Ocean indicate time scales of 1–10 months depending on season and location (e.g., Park et al. 2005). We return in section 2a to a discussion of damping time scales implied by Fig. 1d in the Southern Ocean.

Figure 2 describes the process by which SSTs may be influenced by mesoscale ocean eddies at the sea surface. As the eddies sweep water meridionally (Fig. 2a), anomalously warm (cold) water is moved poleward (equatorward). Mixing and anomalous air–sea fluxes (Fig. 2b) result in the warm water cooling and the cold water warming. Thus a lateral eddy flux of heat through the mixed layer is achieved that is intimately tied to mixing

and anomalous air–sea fluxes induced by the eddies themselves (Fig. 2c). Considering the streamwise average, eddies act to reduce meridional gradients of temperature through both stirring and the modulation of air–sea fluxes, and the gradients are then restored by air–sea interaction acting on the large scales (Fig. 2d). It is this “passive” coupling mechanism that will be investigated in this paper through a kinematic study of an idealized SST-like tracer. Other potential mechanisms for an “active” coupled feedback response involve the dynamical influence of the eddies on the wind stress curl that results from the SST gradients associated with the eddies, as discussed by, for example, Bourras et al. (2004), Spall (2007), Jin et al. (2009), and Hogg et al. (2009).

The modulation of air–sea heat and freshwater fluxes by ocean eddies is likely to be important for the large-scale circulation. For example, theoretical work (Marshall et al. 2002; Radko and Marshall 2004) has indicated a possible role of near-surface diabatic eddy fluxes in the maintenance of the main thermocline, and recent work by Iudicone et al. (2008) has highlighted the role of surface forcings and mixing in water mass formation and transformation in the Southern Ocean. More generally, air–sea interaction with the mesoscale eddy field will likely play an important role in biogeochemical cycles and ecosystem evolution through the influence on the upwelling of dissolved gases and nutrients into the surface ocean.

In this paper, we introduce new diagnostics to characterize the lateral eddy heat flux associated with (i) stirring by eddies and (ii) eddy modulation of air–sea interaction, and we discuss the large-scale implications. The study considers the evolution of an idealized SST-like tracer advected by surface geostrophic velocities derived from altimetric data. The domain considered is the Southern Ocean, and particular attention is given to the influence of eddy processes in the distinct dynamical regimes of the core of the ACC, its flanks, and the region farther equatorward.

The paper is organized as follows: In section 2, we outline the difficulties associated with traditional approaches to quantifying eddy fluxes. In particular, eddy fluxes typically include a (hard to remove) large rotational component that plays no role in the tracer budget (see Marshall and Shutts 1981). Then we set out a new theoretical framework for application to SSTs, based on an extension to the “effective diffusivity” formalism of Nakamura (1996). The effective diffusivity approach focuses on determining the irreversible mixing effect of eddies on tracers, which results from the divergent eddy fluxes. New diagnostics are presented to quantify the effective diffusivity associated with eddy stirring and eddy modulation of air–sea interaction. In section 3, we apply the effective diffusivity formalism to

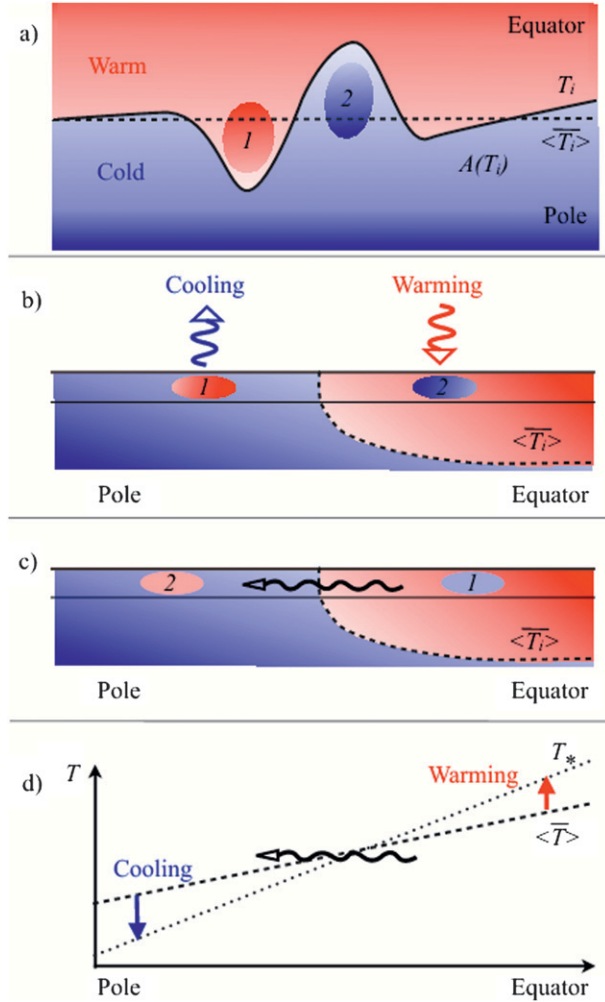


FIG. 2. Schematic diagram of SST fluctuations associated with meandering ocean currents. (a) A temperature contour $T_i = \langle T_i \rangle + T'_i$ is marked (T_i : solid, $\langle T_i \rangle$: dashed), and the area enclosed within that contour $A_i = A(T_i)$ is indicated by blue shading. Eddies (here tracked with labels 1 and 2) sweep anomalously warm (cold) water poleward (equatorward) and then return toward their original latitudes. (b) Mixing of the anomalously warm/cold eddies with the surrounding ocean will reduce the temperature anomaly, as will damping by air-sea interactions. (c) As the modified anomalies return toward their original latitudes (eddy 1 moves equatorward and eddy 2 moves poleward), a lateral eddy flux of heat (wavy line) is supported through the mixed layer. (d) Through repeated action, the eddies thus act to reduce meridional gradients of temperature T , which are then restored to T_* by air-sea interactions on the large scale.

the surface Southern Ocean and quantify/discuss the augmenting effects of eddy stirring and eddy damping by air-sea interaction in determining the lateral eddy diffusivity. In section 4, we discuss the application of our effective diffusivity approach to other fields such as salinity and chlorophyll. Finally, we conclude and discuss the implications of our results in section 5.

2. Theoretical framework

The evolution of the sea surface temperature T can be written as

$$\frac{\partial T}{\partial t} + \nabla \cdot (\mathbf{v}T) = D + F, \quad (1)$$

where \mathbf{v} is the velocity, D is a dissipation term, and F is a forcing term. We will assume that at the surface the flow $\mathbf{v} = (u, v)$ is two dimensional and nondivergent.

a. Traditional approach

Applying the standard Reynolds decomposition to Eq. (1), it is possible to derive an eddy heat variance equation that in steady state is given by (see, e.g., Marshall and Shutts 1981)

$$\nabla \cdot \left(\frac{\overline{\mathbf{v}'T'^2}}{2} \right) + \overline{\mathbf{v}'T'} \cdot \nabla \overline{T} = \overline{D'T'} + \overline{F'T'}, \quad (2)$$

where $\overline{(\cdot)}$ is a time average over a period long compared to that of an eddy. Integrating over the region between contours of $\overline{\Psi}$ (where Ψ is the streamfunction associated with \mathbf{v}) and neglecting the triple correlation term gives

$$\langle \overline{\mathbf{v}'T'} \cdot \nabla \overline{T} \rangle = \langle \overline{D'T'} \rangle + \langle \overline{F'T'} \rangle, \quad (3)$$

where the bracket indicates a spatial average over an area contained within time-mean $\overline{\Psi}$ contours. In the present application we envisage integrating over two closely adjacent $\overline{\Psi}$ contours that thread around Antarctica and so $\langle (\cdot) \rangle$ can also be thought of as a streamwise average.

Let us parameterize the eddy components of the forcing and dissipation as a damping of variance with a rate of $\lambda = \lambda_{\text{total}}$, such that $F' + D' = -\lambda_{\text{total}}T'$, then

$$\lambda_{\text{total}} = -\frac{\langle \overline{\mathbf{v}'T'} \cdot \nabla \overline{T} \rangle}{\langle \overline{T'^2} \rangle}. \quad (4)$$

The damping rate λ_{total} derived in this way is related both to the influence of ocean eddies on the SST and modulation of the air-sea heat flux by eddies (and any other dissipative processes such as entrainment of heat at the base of the mixed layer). Zhai and Greatbatch (2006a) estimated Eq. (4) from satellite altimetry and SST data in the western North Atlantic and found values of 20–30 days in the Gulf Stream and 100 days or longer in less eddy-rich regions. We attempted to estimate the time scale locally (and an eddy diffusivity formulated in a similar manner) directly from the eddying model shown in Fig. 1. The results, however, were highly sensitive to the details of the calculation procedure due largely to

the predominance of rotational fluxes in regions of strong mean-flow advection of temperature variance T'^2 (see discussion in Marshall and Shutts 1981).

Returning to Eq. (1), let us suppose the dissipation D is molecular, turbulent, or subgrid-scale numerical diffusion represented by

$$D = k\nabla^2 T. \quad (5)$$

Let us further suppose the forcing F can be represented as a simple restoring boundary condition to a climatological profile T_* (this is a standard assumption made in models and reflects the dominant physical processes associated with air–sea interaction outlined in the introduction). Following this convention, we set

$$F = -\lambda(T - T_*), \quad (6)$$

where λ is the relaxation (or damping) rate (Haney 1971).

In the context of the surface ocean, the appropriate relaxation profile is a large-scale field determined primarily by the atmospheric forcing. Here, we wish to isolate the effect of the mesoscale ocean eddies on the ocean heat budget. To do so, we take T_* to have the profile of the time-mean streamlines, suitably scaled. We thus neglect the contribution to the air–sea heat flux that arises from the large-scale meanders in the time-mean ACC. We use $\langle(\cdot)\rangle$ to represent an average around a streamline and over time and $(\cdot)'$ to represent the departure from this average, such that $T = \langle\bar{T}\rangle + T'$. Because T_* has the profile of the time-mean streamlines, $T_* = \langle\bar{T}_*\rangle$. Substituting for D and F in Eq. (1), we find

$$\frac{\partial T}{\partial t} + \mathbf{v} \cdot \nabla T = \underbrace{k\nabla^2 T}_{\text{small-scale mixing}} \underbrace{-\lambda T'}_{\text{eddy damping}} \underbrace{-\lambda(\langle\bar{T}\rangle - T_*)}_{\text{large-scale relaxation}}. \quad (7)$$

Here, we have chosen to separate out the term F into an eddy damping term and a large-scale relaxation term, which can be interpreted as the relaxation of the standing meanders of SST in the ACC to those of surface air temperature. Assuming that the eddy damping term is mainly a consequence of air–sea interaction [other possible contributions include, e.g., entrainment at the base of the mixed layer; see Frankignoul (1985) and Zhai and Greatbatch (2006b) for a detailed discussion], the damping rate can be associated with Q' , the anomalous air–sea heat flux, as follows:

$$-\lambda T' = \frac{Q'}{\rho_0 C_p H}. \quad (8)$$

Multiplying Eq. (8) by T' and taking the time and streamline average leads to an estimate of the damping rate λ , which was discussed in the introduction,

$$\lambda = \frac{-1}{\rho_0 C_p H} \frac{\langle Q' T' \rangle}{\langle T'^2 \rangle}. \quad (9)$$

This is the dissipation rate associated with the modulation of the air–sea heat flux by ocean eddies. The maps shown in Fig. 1d give typical values of $\overline{Q' T' / T'^2} = 20\text{--}40 \text{ W m}^{-2} \text{ K}^{-1}$. From this, Eq. (9) yields a damping time scale λ^{-1} on the order of 2–4 months if the mixed layer is 100 m deep.

We now go on to discuss how we propose to use a Nakamura tracer-based framework (Nakamura 1996) to quantify the impact of damping of eddies by air–sea interaction on surface eddy diffusivities.

b. Using a tracer-based framework

Equation (7) can be transformed to a coordinate system based on the area A_i contained within contours $T = T_i$ of the tracer (the area $A_i = A(T_i) = \int_{T \leq T_i} dA$ is represented by the blue shading in Fig. 2a). In this framework, the diffusive effects of the eddies can be clearly identified because only diffusion, not advection, can change the area that a particular tracer contour encloses. We refer the reader to earlier papers (Nakamura 1996; Marshall et al. 2006; Shuckburgh et al. 2009a) and to the appendix for a full explanation and derivation.

In the new coordinate system, Eq. (7) can be rewritten as

$$\frac{\partial T}{\partial t} = \frac{\partial}{\partial A} \left(K_{\text{eff}} \frac{\partial T}{\partial A} \right) - \lambda \frac{\partial}{\partial A} \int (\langle\bar{T}\rangle - T_*) dA, \quad (10)$$

where $K_{\text{eff}} = K_{\text{Nak}} + K_\lambda$ with

$$K_{\text{Nak}} = k \frac{\frac{\partial}{\partial A} \int |\nabla T|^2 dA}{\left(\frac{\partial T}{\partial A}\right)^2} \quad \text{and} \quad (11)$$

$$K_\lambda = \frac{\lambda \int (T') dA}{\frac{\partial T}{\partial A}}. \quad (12)$$

This defines a modified effective diffusivity K_{eff} , which comprises the Nakamura effective diffusivity K_{Nak} (representing the enhancement of the background diffusion k that is generated by eddy stirring) and an additional term K_λ (representing the diffusive effect of the relaxation on the small scales). Because eddies in the flow act to generate small-scale features in the temperature

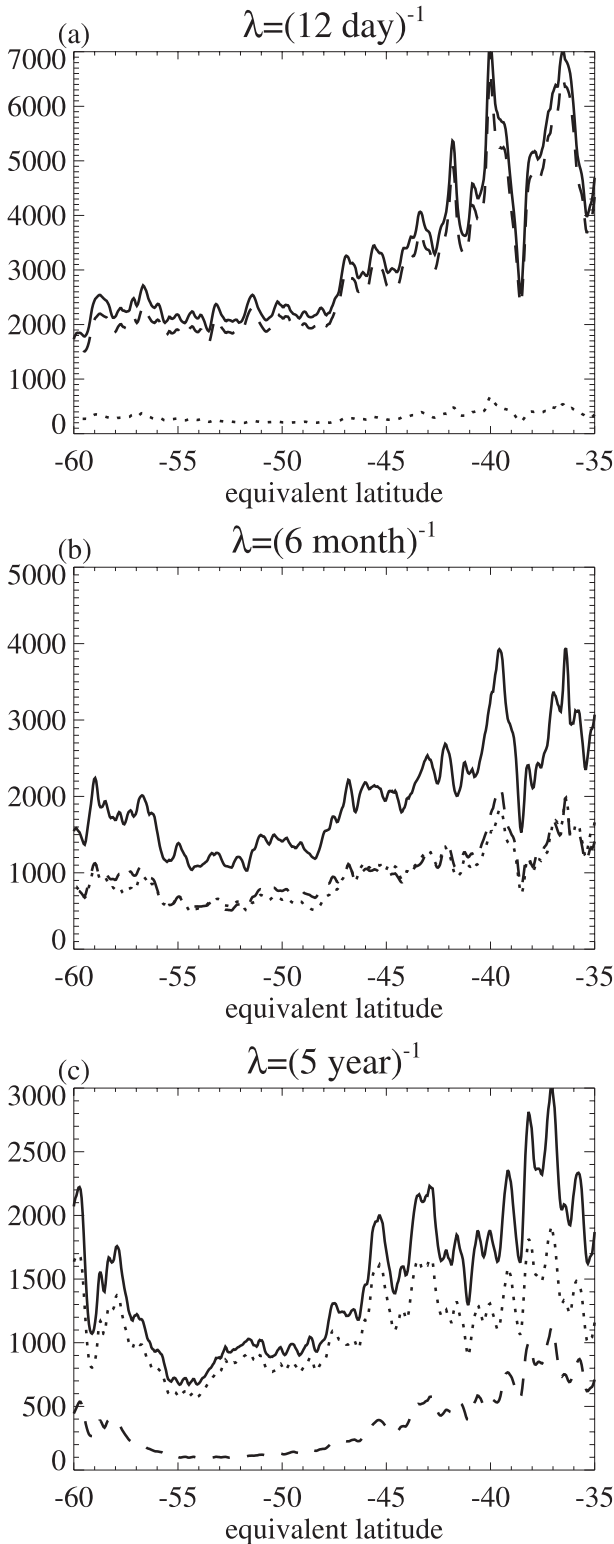


FIG. 3. Latitude dependency of surface eddy diffusivity with K_λ (dashed line), K_{Nak} (dotted line), and $K_{eff} = K_\lambda + K_{Nak}$ (solid line). Results are plotted, at the equilibrium state, for a relaxation time scale of (a) $\lambda^{-1} = 12$ days, (b) 6 months, and (c) 5 yr. (Note the different vertical scales.)

field, the large-scale relaxation profile damps them in a manner much like a diffusion process. When an eddy is advected away from the mean temperature contour, the atmosphere above will tend to dissipate it. In doing so, an additional lateral eddy flux in the ocean’s diabatic surface layer (as indicated in Figs. 2a–c) is introduced. It is evident from Eq. (11) that $K_{Nak} \geq 0$. But what about K_λ ? Consider Fig. 2a. Note the following: (i) as one moves equatorward, T increases and so does $A(T)$ (blue shading), and hence $\partial T/\partial A > 0$; (ii) a positive temperature anomaly (red blob) corresponds to a negative area change, and hence T' and dA are negatively correlated. Thus, $K_\lambda \geq 0$ (and $K_{eff} \geq 0$), as is required of diffusivity. On the large scale, there is a balance between the influence of eddy diffusion acting to flatten tracer gradients and the influence of the relaxation acting to restore them. The final term on the RHS of Eq. (10) is analogous to the last term of (7) and represents the restoring influence of the relaxation to large-scale tracer gradients (as indicated in Fig. 2d).

3. Surface effective diffusivity from altimetric observations

a. Model results

We used the same numerical framework as Marshall et al. (2006) and Shuckburgh et al. (2009a,b) to calculate the surface effective diffusivity. The infrastructure of the Massachusetts Institute of Technology general circulation model (MITgcm; Marshall et al. 1997a) was employed to evolve a tracer according to Eq. (7) with the velocity field \mathbf{v} being the lateral near-surface geostrophic velocity field derived from altimetry data (for more details, see Marshall et al. 2006). A horizontal resolution of $1/20^\circ$ in latitude and longitude was used for the numerical tracer simulation and a value of numerical diffusivity of $k = 50 \text{ m}^2 \text{ s}^{-1}$. In all the integrations to be presented here, the tracer field was initialized with the time-mean streamlines and relaxed back to this profile over a time scale λ^{-1} , which varied from 1 day to 10 yr. The evolving tracer field was output at 10-day intervals, and the effective diffusivity was calculated for each output following Eqs. (11) and (12). A 50-day running mean in time and a $1/4^\circ$ running mean in equivalent latitude were then applied to the effective diffusivity results to remove some of the high-frequency noise arising from the calculation (Shuckburgh et al. 2009a). In the limit of very long relaxation time scale, we set $K_\lambda = 0$ and took K_{Nak} from the results of Marshall et al. (2006), where there was no relaxation of the tracer. For the limit of very short relaxation time scale, the eddies have no time to act before they are damped away, and

the tracer profile will remain close to the relaxation profile. Therefore, we set the eddy diffusivities to their minimum values: that is, $K_\lambda = 0$ and $K_{\text{Nak}} = k$ (the numerical diffusivity) in this limit.

We first verified that the calculation of the effective diffusivity is not strongly sensitive to the chosen value of numerical diffusion k . This has already been shown to be true for the case of no relaxation (Marshall et al. 2006; Shuckburgh et al. 2009a). In the appendix we present the results at equilibrium for a strong relaxation time scale of $\lambda^{-1} = 12$ days with two values of numerical diffusivity, $k = 50 \text{ m}^2 \text{ s}^{-1}$ and $k = 100 \text{ m}^2 \text{ s}^{-1}$. Here, K_λ and K_{Nak} are found to be nearly identical for the two values of k . A similar result was found for other values of the relaxation time scale.

For the case of no relaxation, it was found (Shuckburgh et al. 2009a) that the calculation of K_{Nak} reached an equilibrium value after an initial spinup time of about 3 months for a value of $k = 50 \text{ m}^2 \text{ s}^{-1}$. Those authors noted that this adjustment time was inversely related to the value of the numerical diffusivity. Here, we find that K_λ reaches equilibrium after a time scale of about λ^{-1} . Consequently, we choose to present the results for K_{eff} after an integration of at least 1 yr, with longer integrations for the longer relaxation time scales.¹

The results of calculations at equilibrium for relaxation times of 12 days, 6 months, and 5 yr are shown in Fig. 3 with K_{Nak} (dotted line), K_λ (dashed line), and $K_{\text{eff}} = K_{\text{Nak}} + K_\lambda$ (solid line). The results are plotted against equivalent latitude.²

For short relaxation time scales ($\lambda^{-1} = 12$ days; Fig. 3a), the value of K_{eff} (solid line) is dominated by the contribution from K_λ (dashed line), whereas, for long relaxation time scales ($\lambda^{-1} = 5$ yr; Fig. 3c), the value of K_{eff} is dominated by the contribution from K_{Nak} (dotted line). For $\lambda^{-1} = 6$ months (Fig. 3b), K_{Nak} and K_λ provide approximately equal contributions to K_{eff} .

Figure 4a presents the results of effective diffusivity for various values of the relaxation time. The results are averaged over the equivalent latitude bands used by Shuckburgh et al. (2009a), which are representative of the core of the ACC (49°–56°S, black line), the flanks of the ACC (41°–49°S, dark gray line), and equatorward of the ACC (33°–41°S, light gray line). In each band, the

¹ For these calculations, we used altimetry data from 1997, annually repeating where required.

² The equivalent latitude, $\phi_e(T, t)$, is related to the area A within a tracer concentration contour by the identity $A = 2\pi r^2(1 - \sin\phi_e)$, with r being the radius of the earth. For each tracer contour, the equivalent latitude is therefore the latitude the contour would have if it were remapped to be zonally symmetric while retaining its internal area.

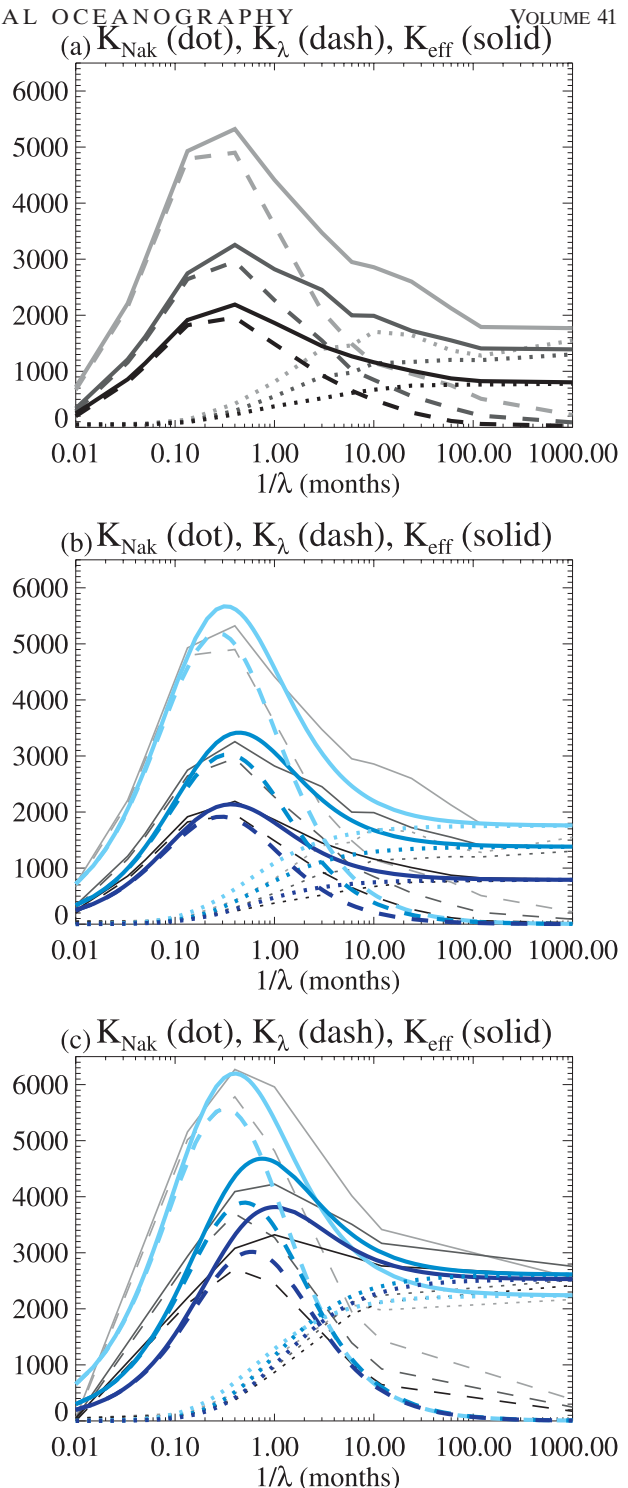


FIG. 4. Dependency of surface eddy diffusivity on relaxation time scale inferred from the tracer analysis averaged over the equivalent latitude bands: K_{Nak} (dotted lines), K_λ (dashed lines), and $K_{\text{eff}} = K_{\text{Nak}} + K_\lambda$ (solid lines). (a) Results for three equivalent latitude bands: 33°–41°S (light gray lines), 41°–49°S (dark gray lines), and 49°–56°S (black lines). (b) Overplotted in blue are the results of the analytical estimate of K_{eff} given by Eq. (18). (c) The results for a calculation where the mean flow is set to 0 (i.e., the flow field consists only of the eddies).

values of $K_{\text{eff}} = K_{\text{Nak}} + K_{\lambda}$ show a maximum at approximately $\lambda^{-1} = 10$ days and the values of K_{Nak} and K_{λ} are found to be equal in each band at a relaxation time of approximately 200 days.

b. Scaling of effective diffusivity with damping time-scale and flow-field parameters

We now explore how K_{eff} may be expected to vary with the damping rate λ and flow-field parameters. Previous studies (Shuckburgh et al. 2001; Marshall et al. 2006) have argued that in mixing regions the Nakamura effective diffusivity is expected to scale as SL_{eddy}^2 , where S is the stretching rate of the flow and L_{eddy} is the typical size of an eddy mixing region. Thus, in the limit $\lambda \rightarrow 0$, we would anticipate $K_{\text{eff}} \rightarrow K_{\text{Nak}}(0) = SL_{\text{eddy}}^2$. In the limit $\lambda \rightarrow \infty$, we would anticipate $K_{\text{eff}} \rightarrow k$, because the eddies have no opportunity to act before being damped away. For simplicity, we consider here only the regime in which K_{eff} is at least an order of magnitude greater than k . In this case, we can approximate the limit of large λ by $K_{\text{eff}} \rightarrow 0$.

Guided by Eqs. (3), (5), and (6) and assuming a local down-gradient closure with an eddy diffusivity $K = K_{\text{total}}$ to represent the eddy heat flux, $K_{\text{total}} \nabla \overline{T} = -\overline{\mathbf{v}'T'}$, we suggest the eddy diffusivity may be estimated as

$$K_{\text{eff}}(\lambda) = K_{\lambda}(\lambda) + K_{\text{Nak}}(\lambda) \sim K_{\text{total}}(\lambda) \sim \frac{\lambda \langle \overline{T'^2} \rangle}{\langle |\nabla \overline{T}|^2 \rangle} - \frac{k \langle \overline{T' \nabla^2 T'} \rangle}{\langle |\nabla \overline{T}|^2 \rangle}. \quad (13)$$

Tracer stirring by eddies will create gradients on the Batchelor scale, $\delta = \sqrt{k/S}$ (Marshall et al. 2006). We therefore expect $K_{\text{Nak}}(\lambda)$ to scale as (see Plumb 1979)

$$K_{\text{Nak}}(\lambda) \sim \frac{-k \langle \overline{T' \nabla^2 T'} \rangle}{\langle |\nabla \overline{T}|^2 \rangle} \sim \frac{k \langle \overline{T'^2} \rangle}{\delta^2 \langle |\nabla \overline{T}|^2 \rangle} \sim \frac{S \langle \overline{T'^2} \rangle}{\langle |\nabla \overline{T}|^2 \rangle}. \quad (14)$$

Thus, writing $K_{\text{Nak}}(\lambda) = a(S \langle \overline{T'^2} \rangle / \langle |\nabla \overline{T}|^2 \rangle)$, where a is an $O(1)$ scaling factor, we can rearrange Eq. (13) to give

$$K_{\text{eff}}(\lambda) \sim (\lambda + aS) \frac{\langle \overline{T'^2} \rangle}{\langle |\nabla \overline{T}|^2 \rangle}. \quad (15)$$

Now, if $K_{\text{Nak}}(\lambda = 0) = a(S \langle \overline{T_0'^2} \rangle / \langle |\nabla \overline{T_0}|^2 \rangle)$, where the subscript 0 in T_0 indicates the case $\lambda = 0$, and if we assume $\overline{\mathbf{v}'T_0} \sim \nabla \overline{T}$, then we can rewrite Eq. (15) as

$$K_{\text{eff}}(\lambda) \sim \frac{\lambda + aS}{aS} \frac{\langle \overline{T'^2} \rangle}{\langle \overline{T_0'^2} \rangle} K_{\text{Nak}}(0). \quad (16)$$

To proceed further, we need to scale the ratio $\langle \overline{T'^2} \rangle / \langle \overline{T_0'^2} \rangle$. We expect the SST anomalies to be weaker

in the presence of air–sea damping. However, we also expect this effect to be significant only for damping time scales of the order of or shorter than the time scale τ over which filaments are generated. As the simplest possible scaling let us write

$$T' = \frac{T'_0}{(1 + \lambda\tau)}. \quad (17)$$

This simply states that, for weak damping, air–sea interaction does not affect SST variance and $T' \sim T'_0$, whereas, for strong damping, SST anomalies (and SST variance) become vanishingly small. In other words, for $\lambda^{-1} \gg \tau$, water parcels are moved back and forth without “feeling” the air–sea flux and thus without exchanging any heat with the atmospheric boundary layer. The time scale τ is best thought of as an advection time scale that takes into account the effect of eddies or more precisely the Lagrangian decorrelation time scale. For short damping time scales $\lambda^{-1} \ll \tau$, SST anomalies are strongly damped before advection can effectively stir them, and the effective diffusivity is anticipated to increase with λ^{-1} (Pasquero 2005).

The scaling of $\langle \overline{T'^2} \rangle / \langle \overline{T_0'^2} \rangle$ can be related to the Damköhler number $\text{Da} = \lambda\tau$ (Pasquero 2005; Kramer and Keating 2009), which relates the advection time scale to the reaction time scale (which here is the relaxation–damping time scale). It seems plausible that the maximum value of K_{λ} should correspond to a time scale between the two limits described above, when value of λ^{-1} is equal to the Lagrangian decorrelation time scale τ (i.e., $\text{Da} = 1$). Putting (17) and (16) together, we obtain the following:

$$K_{\text{eff}}(\lambda) \sim \frac{\lambda + aS}{aS} (1 + \lambda\tau)^{-2} K_{\text{Nak}}(0). \quad (18)$$

The first thing to note is that this scaling does not depend on the diffusivity k , in agreement with our findings. In Eq. (18), we know (approximately) S and τ , which are properties of the eddy flow, whereas $K_{\text{Nak}}(0)$ was computed in Marshall et al. (2006). The coefficient a is the only fitting parameter.

Equation (18) predicts the following (see Figs. 4b,c for illustration): (i) K_{eff} will converge to $K_{\text{Nak}}(0)$ for large λ ; (ii) K_{eff} becomes very small for small λ (in this limit the damping is so strong that the eddy field cannot deform the mean SST contours and thus create filaments); and (iii) between these two limits, K_{eff} peaks at a damping time scale of $\lambda_p^{-1} = \tau / (1 - 2S\tau)$, with the peak value being dependent on $K_{\text{Nak}}(0)$, S , and τ . This can be interpreted as follows: For somewhat weak damping ($\lambda^{-1} \geq \lambda_p^{-1}$), the

SST variance is mainly generated by the chaotic advection of the eddy field, and the air–sea heat flux provides, alongside the small-scale mixing, an additional mechanism to destroy variance; hence, the effective diffusivity increases above $K_{\text{Nak}}(0)$. As the strength of the damping increases, the SST variance is reduced, hampering the ability of the eddy fields to generate filaments. Ultimately, for very large damping, the SST field is “pinned down” to T_* , the eddy field cannot create SST anomalies, $T' \rightarrow 0$, and the eddy diffusivity converges to k .

The stretching rate S can be estimated from a calculation of finite-time Lyapunov exponents (Marshall et al. 2006). The results for the three equivalent latitude bands are $S = 2.13 \text{ month}^{-1}$ for the ACC, 2.01 month^{-1} for the flanks of the ACC, and 1.88 month^{-1} equatorward of the ACC. We take the value of τ as the damping time scale at which K_λ peaks and this gives values of $\tau = 0.29$ (ACC), 0.34 (flanks), and 0.27 month (equatorward). These values, which are in the range 8–10 days, are broadly consistent with the Lagrangian decorrelation times found by Veneziani et al. (2004) for the northwest Atlantic. The presence of coherent structures in the flow (meandering jets and vortices) alters the decorrelation time, making it longer where trajectories exhibit looping (Richardson 1993). This likely explains the slightly larger value of τ found on the flanks of the ACC.

These S and τ values are used to estimate the values of K_{Nak} , K_λ , and K_{eff} according to Eq. (18) with $a = 1/6$. The results are presented in Fig. 4b as blue curves. It can be seen that the estimate provides a remarkably good fit to the diffusivities.

As a final test of the scaling, we consider the case where the tracer is advected only by eddies with the mean flow set to zero. The stretching rate, which scales with the eddy kinetic energy (EKE; Waugh et al. 2006), is expected to remain similar. On the other hand, the typical Lagrangian decorrelation time τ may be expected to be 1) longer, because of the presence of more looping trajectories,³ and 2) more uniform across the latitude bands, because of the absence of the influence of jets in some regions. The results for the effective diffusivities in the case of no mean flow are presented in Fig. 4c. Marshall et al. (2006) found that the Nakamura effective diffusivity [$K_{\text{Nak}}(0)$] in this case varied little in latitude. Consistent with this, K_{Nak} [which we suggest scales only with $K_{\text{Nak}}(0)$ and τ] is seen to be similar for

each of the latitude bands. The maximum values of K_λ and K_{eff} are shifted to longer damping times. Again, taking the value of τ as the damping time scale at which K_λ peaks, we find values of $\tau = 0.32$ (ACC), 0.5 (flanks), and 0.59 month (equatorward). This is consistent with the anticipated longer Lagrangian decorrelation time without the mean flow. When we use these values of τ to reestimate the values of K_{Nak} , K_λ , and K_{eff} according to Eq. (18), we again find a good fit (blue curves in Fig. 4c). This further confirms the utility of our scaling.

We now use Eq. (18) to estimate the values of K_{eff} of relevance to the Southern Ocean. We take representative values for the stretching rate and Lagrangian decorrelation time scales of $S = 2 \text{ month}^{-1}$ and $\tau = 0.3$ month. For the damping time scale λ^{-1} , we take values in the range 2–8 months. Because we expect a shorter damping time scale in regions of strong eddy activity, we use the streamwise average of $(\text{EKE})^{-1}$ to set the spatial variability within this range (using 10 times the value of EKE in $\text{m}^2 \text{ s}^{-2}$ gives a value of λ in months^{-1} of about the right magnitude). The EKE is largest on the flanks of the ACC (with an average value of $0.029 \text{ m}^2 \text{ s}^{-2}$) and this gives an average value of our estimated λ^{-1} of 3.83 months. Equatorward the average value of EKE is smaller ($0.017 \text{ m}^2 \text{ s}^{-2}$), and this gives an average value of λ^{-1} of 5.97 months.

The results for 16 October 1998⁴ are presented in Fig. 5a. The effective diffusivity calculated for a “conserved tracer” (by which we mean a tracer for which the reaction rate λ is zero) as in Shuckburgh et al. (2009a) is plotted for comparison in Fig. 5b (black curve). As previously, a smoothing has been applied to remove unrealistic high-frequency noise. The latitudinal distribution for the total effective diffusivity for SST and the conserved tracer are very similar with low values in the core of the ACC and higher values equatorward. The values for SST are typically about $500 \text{ m}^2 \text{ s}^{-1}$ larger than those for a conserved tracer, ranging from about 1500 to over $3000 \text{ m}^2 \text{ s}^{-1}$. In the core of the ACC, K_{Nak} and K_λ contribute about equally to the total effective diffusivity, whereas equatorward K_{Nak} contributes about two-thirds and K_λ contributes about one-third. The values of K_{eff} for SST are broadly in line with those found by Zhai and Greatbatch (2006a). They found values in the range 1000 – $2000 \text{ m}^2 \text{ s}^{-1}$ within the Gulf Stream, with some “hot spots” of $10^4 \text{ m}^2 \text{ s}^{-1}$ to the south. Although we do not find such large hot spots, it should be remembered that our values are a streamwise average. It

³ Veneziani et al. (2004) found significantly more looping trajectories and longer decorrelation times north of the Azores current, where there is only a weak eastward mean flow.

⁴ Note that the diffusivity calculated for this day will reflect the influence of the eddies on the tracer field over the recent past defined by some memory time. See appendix for further details.

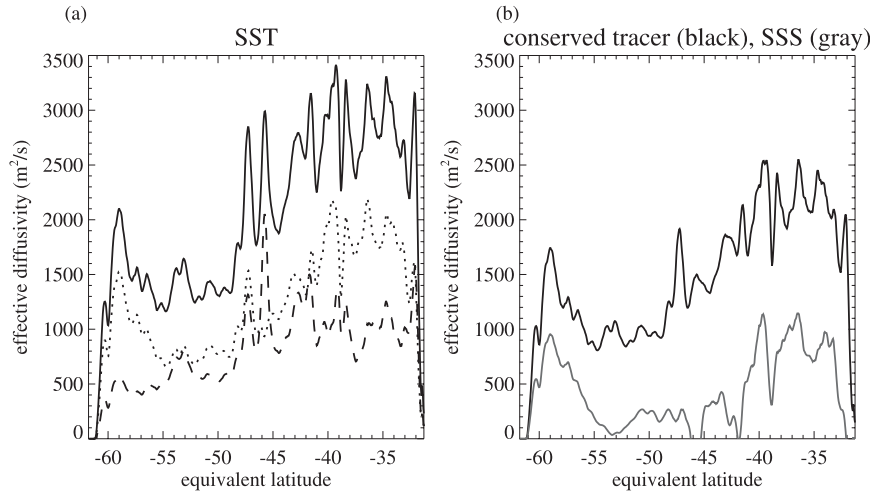


FIG. 5. Effective diffusivity for 16 Oct 1998 (a) for SST, with K_{Nak} (dotted line), K_{λ} (dashed line), and $K_{\text{eff}} = K_{\text{Nak}} + K_{\lambda}$ (solid line), and (b) for a conserved tracer (black line) and SSS (gray line), both with K_{eff} .

should also be noted that our values represent a minimum effective diffusivity, because they do not account for, for example, interactions at the base of the mixed layer.

Finally, Fig. 6 presents the values of K_{eff} calculated for Fig. 5a, plotted on the relevant equivalent latitude contours. This figure is to be compared with the results of the Nakamura effective diffusivity for a conserved tracer presented in Fig. 1 of Shuckburgh et al. (2009a). The same basic pattern of low values in the ACC and higher values on its flanks can be clearly observed in both cases.

4. Effective diffusivity for other tracers

We now consider the relevance of our results for other tracer fields: namely, sea surface salinity (SSS), phytoplankton, zooplankton, and various dissolved gases.

a. Salinity

The case of sea surface salinity (SSS) is particularly interesting because, as described below, our results suggest that, depending on the relative directions of the temperature and salinity gradients, air–sea interaction could enhance or diminish the effective eddy diffusivity of salinity. Returning to Fig. 2, consider the case where temperature and salinity gradients are in the same direction (as in the ACC, where both point equatorward). As a warm and salty water parcel moves southward, it experiences a cooling, partly achieved through latent heat flux–evaporation. Hence, although temperature anomalies are damped, salinity anomalies are reinforced, generating an up-gradient flux as they return northward.

Thus, we expect that, in such a case, K_{λ}^S for salt would be negative. If, however, temperature and salinity gradients are opposed to one another (as in the subtropics), K_{λ}^S is expected to be positive.

Making some simple approximations, the term in the salinity variance equation associated with freshwater exchanges at the air–sea interface can be expressed in a form analogous to that seen in the temperature case. This in turn allows us to relate the air–sea eddy diffusivity of salt K_{λ}^S to that of temperature K_{λ}^T .

Let us start by considering again the case of temperature. Equation (7) can be used to generate a variance temperature equation, in which the relevant terms are

$$\frac{\partial}{\partial t} \left(\frac{\langle T'^2 \rangle}{2} \right) + \dots = -\lambda_T \langle T'^2 \rangle + \dots, \quad (19)$$

with λ_T being the damping time scale for temperature given by Eq. (8). In a similar way, a variance salinity equation can be written, in which the relevant terms are

$$\frac{\partial}{\partial t} \left(\frac{\langle S'^2 \rangle}{2} \right) + \dots = \frac{S_O}{\rho_F H} (\langle E'S' \rangle - \langle P'S' \rangle) + \dots, \quad (20)$$

where E' and P' are the evaporation and precipitation anomalies (in $\text{kg m}^{-2} \text{s}^{-1}$), S_O is the reference salinity, and ρ_F is the freshwater density.

The evaporation anomaly is proportional to the latent heat anomaly, $Q'_L = -L_w E'$, where L_w is the latent heat of vaporization ($=2.5 \times 10^6 \text{ J kg}^{-1}$). From Eq. (8), the latent heat contribution can be written as

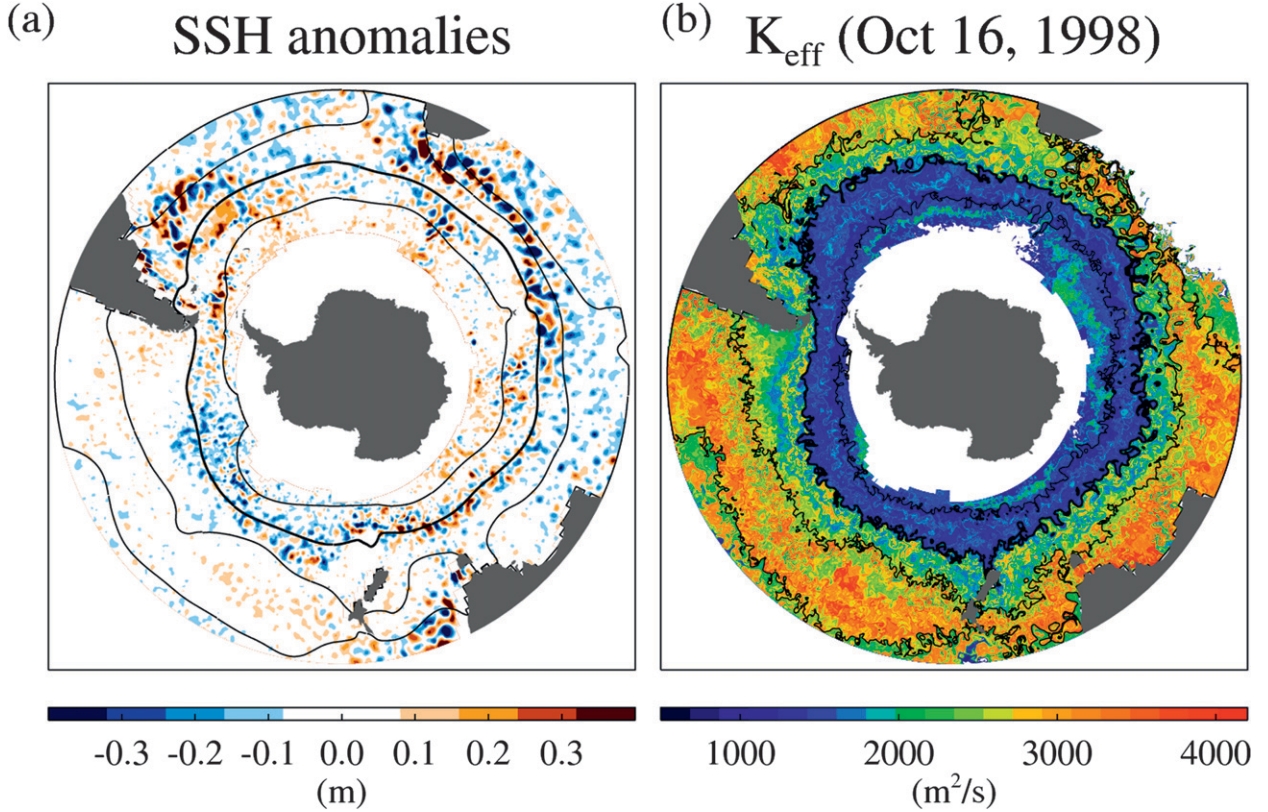


FIG. 6. (a) Sea surface height (SSH) anomalies and (b) effective diffusivity $K_{\text{eff}}(\phi_e)$ for SST for 16 Oct 1998 with overplotted streamlines with values (from equator to pole) of -9 , -5 , 0 (bold), and $6 \times 10^4 \text{ m}^2 \text{ s}^{-1}$ [time-mean streamlines in (a), instantaneous streamlines in (b); these mark the equivalent latitude bands used to denote the ACC, its flanks, and equatorward]. Note that K_{eff} is a function of equivalent latitude ϕ_e only; therefore this two-dimensional plot contains only one-dimensional information (see text for further explanation). Latitudes from 30°S to the pole are plotted.

$$\frac{Q'_L}{\rho_O C_p H} = -\lambda_L T'. \quad (21)$$

The variance equation then becomes

$$\frac{\partial}{\partial t} \left(\frac{\langle S'^2 \rangle}{2} \right) + \dots = \frac{S_O \alpha_L}{\rho_F H L_w} \langle \overline{T' S'} \rangle - \frac{S_O}{\rho_F H} \langle \overline{P' S'} \rangle + \dots, \quad (22)$$

where $\alpha_L = \lambda_L \rho_O C_p H$ is the damping rate ($\text{W m}^{-2} \text{K}^{-1}$) due to latent heat fluxes.

Using mixing length arguments, the SSS and SST anomalies can be related to their large-scale mean gradients; thus,

$$\left. \begin{aligned} T' &= L_m \partial_y \langle \overline{T} \rangle \\ S' &= L_m \partial_y \langle \overline{S} \rangle \end{aligned} \right\} \Rightarrow T' = \frac{\partial_y \langle \overline{T} \rangle}{\partial_y \langle \overline{S} \rangle} S'. \quad (23)$$

Note that the mixing length L_m does not appear here, provided that reasonably it is the same for temperature

and salinity. Finally, we neglect the correlation $\overline{P' S'}$ between precipitation and salinity.⁵ The salinity variance equation can then be written as

$$\frac{\partial}{\partial t} \left(\frac{\langle S'^2 \rangle}{2} \right) + \dots = \frac{S_O \alpha_L}{\rho_F H L_w} \frac{\partial_y \langle \overline{T} \rangle}{\partial_y \langle \overline{S} \rangle} \overline{S'^2} + \dots. \quad (24)$$

From this, by analogy with Eq. (19), we can define a damping time scale for salinity variance as

$$\lambda_S = -\frac{S_O \alpha_L}{\rho_F H L_w} \frac{\partial_y \langle \overline{T} \rangle}{\partial_y \langle \overline{S} \rangle}. \quad (25)$$

This is negative if temperature and salinity gradients are of the same sign, because in this case the salinity

⁵ Because part of the anomalous evaporation is rained out locally, $\langle \overline{P' S'} \rangle$, albeit small, might not be zero. This would slightly counteract the effect of $\langle \overline{E' S'} \rangle$. In the (unlikely) limit that all evaporation is precipitated locally, the air-sea term in the salinity variance would vanish and the salinity and temperature effective diffusivity would still be expected to be different.

variance is increased by the latent heat flux damping of SST anomalies. This is consistent with the heuristic reasoning given at the start of this section.

Consistent with our scaling argument in Eq. (13), we expect the air–sea diffusivity to scale as

$$K_\lambda(\lambda) = \frac{\lambda \langle T'^2 \rangle}{\langle |\nabla T|^2 \rangle} \sim \lambda L_m^2 \quad (26)$$

and the ratio of the air–sea eddy diffusivity for salt and temperature to scale as

$$\frac{K_\lambda^S}{K_\lambda^T} \sim \frac{\lambda_S}{\lambda_T} = -\frac{\rho_O S_O C_p \partial_y \langle \bar{T} \rangle \lambda_L}{\rho_F L_w \partial_y \langle \bar{S} \rangle \lambda_T}. \quad (27)$$

Usefully, the mixed layer depth does not appear. The only uncertain coefficient is the ratio of the latent heat flux damping to the total heat flux damping, $\lambda_L/\lambda_T = \alpha_L/\alpha_T$ (where $\alpha_T = \rho_O C_p H \lambda_T$).

The value of α_L/α_T is not known for the Southern Ocean. However, Frankignoul and Kestenare (2002) estimated for the Northern Hemisphere that the radiative contribution to the total heat flux damping is small, typically less than 10%, and can be neglected. Observations for the Northern Hemisphere also suggest that the ratio of the sensible to the latent heat fluxes, the Bowen ratio, ranges from $1/4$ in midlatitudes to 1 at high latitudes. Overall, this suggests that $\alpha_L/\alpha_T \simeq 0.5$ – 0.8 . Let us assume $\alpha_L/\alpha_T \simeq 0.65$ and that $S_O = 34$ psu and $C_p = 4000 \text{ J kg}^{-1} \text{ K}^{-1}$ (and, of course, $\rho_O/\rho_F \simeq 1$). Typically, $\partial_y \bar{T} = 0.6 \text{ K } (^\circ)^{-1}$ and $\partial_y \bar{S} = 0.02 \text{ psu } (^\circ)^{-1}$, giving a ratio of 30 K psu^{-1} . This gives $K_\lambda^S \sim -K_\lambda^T$ and K_λ^S is <0 .

It should be emphasized that, because of the contribution of K_{Nak}^S , this does not imply that the total effective diffusivity for salt, $K_{\text{eff}}^S = K_{\text{Nak}}^S + K_\lambda^S$, is negative. Assuming the influence on T – S of the stirring by eddies is the same, $K_{\text{Nak}}^S = K_{\text{Nak}}^T$. Then, as long as the magnitude of K_{Nak} is greater than that of K_λ , the total diffusivity for S will be positive. However, our results imply that, near the surface, the effective eddy diffusivity for salt and temperature can be very different, with K_{eff}^S likely less than K_{eff}^T . The eddy diffusivity for SSS, assuming the estimate of $K_\lambda^S = -K_\lambda^T$ from Eq. (27) and adopting the value of K_{Nak} estimated for SST, is given in Fig. 5b (gray curve). The values range from $K_{\text{eff}}^S = 200 \text{ m}^2 \text{ s}^{-1}$ or less in the ACC to $800 \text{ m}^2 \text{ s}^{-1}$ equatorward, considerably smaller than for K_{eff}^T .

b. Biogeochemistry

Our results also have relevance for simple descriptions of biogeochemical processes in the ocean. A number of studies have emphasized the importance of horizontal eddy stirring in determining the surface distribution of,

for example, phytoplankton (Lévy 2003) and the partial pressure of carbon dioxide at the sea surface ($p\text{CO}_2$; Resplandy et al. 2009). Equation (7) has been used to model the carrying capacity field in a simple system describing the evolution of phytoplankton and zooplankton (Abraham 1998), where the carrying capacity is the maximum phytoplankton concentration attainable within a fluid parcel in the absence of grazing. This carrying capacity is assumed to represent the effect of a limiting nutrient or to represent variations in mixed layer depth. As a parcel moves through the domain, the carrying capacity continually relaxes toward a spatially varying background nutrient value, which may be determined by, for example, mixed layer entrainment or wind-driven upwelling. Abraham (1998) took the relaxation profile to be a smooth function of latitude, similar to the relaxation profile used in this study. In both cases, spatial variability is injected into the model at the large scale. Further, Bracco et al. (2009) have used equations of the form of (7) with different values of the relaxation time scale λ^{-1} as a simple description of the evolution of the phytoplankton and zooplankton to understand the structure of their spatial distributions. Mahadevan and Archer (2000) have also used similar expressions to consider tracers such as dissolved organic carbon (DOC) and hydrogen peroxide (including the effect of vertical transport).

Bracco et al. (2009) assumed a value of $\lambda^{-1} = 4$ days for phytoplankton, 12 days for zooplankton, and 40 days for SST (a value broadly in line with the values we have used above), Mahadevan and Archer (2000) used a long relaxation time scale (60 days) for DOC and a short time scale (3 days) for hydrogen peroxide. Considering the results presented in Fig. 4, it can be seen that the values of eddy diffusivity for $\lambda^{-1} = 4$ days (phytoplankton) are close to those for $\lambda^{-1} = 12$ days (zooplankton), with both being strongly dominated by the values of K_λ . This is consistent with the finding of Bracco et al. (2009) that the addition of turbulent diffusion does not significantly modify the spectral slope of tracers with reaction times shorter than the Lagrangian decorrelation time scale. On the other hand, for the longer reaction time scales of relevance to SST, turbulent diffusion was observed by Bracco et al. (2009) to influence the spectral slope, consistent with our finding of a significant contribution by K_{Nak} to the total effective diffusivity. From Fig. 3a, it can be seen that the values of K_{eff} of relevance to phytoplankton or zooplankton range from about $2000 \text{ m}^2 \text{ s}^{-1}$ in the ACC to about $5000 \text{ m}^2 \text{ s}^{-1}$ equatorward.

5. Conclusions and discussion

In this paper, we have presented a new technique that is able to robustly quantify the effective eddy diffusivity

for tracers subject to advection, diffusion, and a simple reaction consisting of a relaxation to a large-scale background profile. The effective diffusivity is expressed as a streamwise average. We have chosen to relax the tracer back to a profile that is aligned with the time-mean streamlines. This assumption will be valid when the time scale for along-stream advection is shorter than the relaxation time scale. This is evidently true for the Southern Ocean, where the mean SST contours are observed to be broadly aligned with the mean streamlines.

We find, for example, that air–sea damping can augment the lateral diffusivity within the mixed layer by, depending on the assumed SST damping time scale, a value on the order of $500 \text{ m}^2 \text{ s}^{-1}$ (see Fig. 5). In frontal regions such as the Gulf Stream, Kuroshio, or ACC, where SST can change on the order of 5°C in 100 km, this is equivalent to an air–sea flux of 100 W m^{-2} acting over a mixed layer depth of 100 m. This is a very significant flux, which would be absent in coarse-resolution models unless explicitly accounted for. Our results may therefore help inform model parameterizations thus improving the fidelity of coarse-grained models.

Our results indicate that, near the surface, the total eddy diffusivities associated with different tracers (e.g., temperature, salinity, dissolved gases, and chlorophyll) may differ significantly in magnitude. We find values in the ACC ranging from about $200 \text{ m}^2 \text{ s}^{-1}$ or less for salinity, through $1500 \text{ m}^2 \text{ s}^{-1}$ for temperature, up to about $2000 \text{ m}^2 \text{ s}^{-1}$ for chlorophyll. The values equatorward of the ACC are larger, but strong differences between tracer species remain with the total eddy diffusivity being $\sim 800 \text{ m}^2 \text{ s}^{-1}$ for salinity, $\sim 3000 \text{ m}^2 \text{ s}^{-1}$ for temperature, and $\sim 5000 \text{ m}^2 \text{ s}^{-1}$ for chlorophyll. This has implications for model parameterizations as it suggests that, near the surface, different values of eddy diffusivity may be required for different tracers.

The approach we have presented in this paper evidently neglects many physical, chemical, and biological processes that may influence surface fields. Nevertheless, it constitutes a powerful new technique that quantifies the mixed layer lateral eddy fluxes mediated by air–sea interaction. In this way, it can be used to provide valuable information concerning the evolution of any surface field (from observations or models) that exhibits variability correlated with the mesoscale eddy field and that is influenced by air–sea interactions.

Acknowledgments. EFS has been supported by an NERC postdoctoral fellowship. The MIT group would like to acknowledge support of both NSF (Physical Oceanography) and NASA (ECCO2).

APPENDIX

Model and Method Description

The eddy-resolving model used was the MITgcm (Marshall et al. 1997a,b). The simulation was conducted as a part of the Estimating the Circulation and Climate of the Ocean, Phase II (ECCO2) project and is freely available on the Internet (available online at <http://ecco2.org>). The ocean is forced from April 2002 to March 2005 by the National Centers for Environmental Prediction (NCEP) Reanalysis-1surface atmospheric state (Kalnay et al. 1996). Sea surface heat fluxes are computed using a classic set of bulk formulas (Large and Yeager 2004). A surface relaxation to monthly Levitus sea surface salinity is applied with a relaxation time constant of 44.5 days (Levitus and Boyer 1994). The simulation also includes a full dynamic–thermodynamic sea ice model (for more details, see online at <http://mitgcm.org>). The resolution of the model is 50 vertical levels and $1/8^\circ$ both in latitude and longitude: that is, about 14 km at the equator decreasing to about 7 km at high latitudes. The model is run globally but the domain of analysis for this study was limited to the Southern Ocean from 20° to 80°S . The model eddy temperature variance field follows the distribution of the eddy kinetic energy because of the mesoscale activity of the Southern Ocean. It is realistically maximum (values from 6° to 10°C^2) south of the Cape of Good Hope (on the poleward flank of the Agulhas current), downstream of the Drake Passage (where the ACC merges with the Brazilian Current in the South Atlantic subtropical gyre southwest corner), along the Brazilian Current off the South American coast, eastward of the New Zealand north coasts, and finally all along the ACC path.

Effective diffusivity derivation

The key to deriving the effective diffusivity is to note that the area enclosed within a tracer contour cannot be changed by advection. Hence, following Nakamura (1996) and using Eq. (7),

$$\begin{aligned} \frac{\partial}{\partial t} A(T, t) &= -\frac{\partial A}{\partial T} \left(\widehat{\frac{\partial T}{\partial t}} \right) \\ &= -\frac{\partial}{\partial T} \int [k\nabla^2 T - \lambda T' - \lambda(\overline{T}) - T_*] dA, \end{aligned} \quad (\text{A1})$$

where $\widehat{(\cdot)}$ is an average of a scalar quantity and is given by

$$(\cdot) \equiv \frac{\partial}{\partial A} \int (\cdot) dA. \quad (\text{A2})$$

This allows the equation for the temporal evolution of the tracer to be written in area coordinates,

$$\begin{aligned} \frac{\partial}{\partial t} T(A, t) &= -\frac{\partial T}{\partial A} \frac{\partial A}{\partial t} \\ &= \frac{\partial}{\partial A} \int [k \nabla^2 T - \lambda T' - \lambda (\langle \overline{T} \rangle - T_*)] dA. \end{aligned} \quad (\text{A3})$$

It has been demonstrated previously (Nakamura 1996; Shuckburgh and Haynes 2003; Marshall et al. 2006) that the first term on the RHS can be written in the form of a diffusive term, with a diffusivity given by

$$K_{\text{Nak}} = \frac{\widehat{|\nabla T|^2}}{(\partial T / \partial A)^2}. \quad (\text{A4})$$

Thus, Eq. (7) can be written as

$$\frac{\partial T}{\partial t} = \frac{\partial}{\partial A} \left(K_{\text{Nak}} \frac{\partial T}{\partial A} \right) - \lambda \widehat{T'} - \lambda (\langle \overline{T} \rangle - T_*). \quad (\text{A5})$$

The term $-\lambda \widehat{T'}$ can then be rewritten in the form of a diffusive term, as in Eq. (10).

Previous studies (Marshall et al. 2006; Shuckburgh et al. 2009a) have investigated dependence of the Nakamura effective diffusivity on the value of the diffusivity k . The results indicated that, when the Péclet number ($\text{Pe} = SL_{\text{eddy}}^2/k$, where S is a stretching rate and L_{eddy} is the typical size of an eddy) is large ($\text{Pe} \geq 50$), then the effective diffusivity is not strongly dependent on k . For calculations with a horizontal resolution of $1/20^\circ$ it was found that the most suitable choice of diffusivity was $k = 50 \text{ m}^2 \text{ s}^{-1}$.

Here, we investigate the dependence of $K_{\text{eff}}(\lambda, k) = K_{\text{Nak}}(\lambda, k) + K_\lambda(\lambda, k)$ on the value of k . In the limit of small λ , then $K_{\lambda,k} \rightarrow 0$ and the above result concerning the independence of the effective diffusivity on the value of k holds. We therefore investigate the case of large λ .

In Fig. A1, we present the results at equilibrium for a strong relaxation time scale of $\lambda^{-1} = 12$ days with two values of numerical diffusivity $k = 50 \text{ m}^2 \text{ s}^{-1}$ (black line) and $k = 100 \text{ m}^2 \text{ s}^{-1}$ (gray line). It can be seen that the results for K_λ (dashed line) and K_{Nak} (dotted line) are nearly identical for the two values of k . A similar result is found for other values of the relaxation time scale. We conclude that K_{eff} is not strongly dependent on the value of the numerical diffusivity for small enough values of k and thus that we can consider $K_{\text{eff}} = K_{\text{eff}}(\lambda)$, $K_{\text{Nak}} = K_{\text{Nak}}(\lambda)$, and $K_\lambda = K_\lambda(\lambda)$.

In a flow with time-varying eddy diffusivity, the geometric structure of a tracer at any instant will depend on

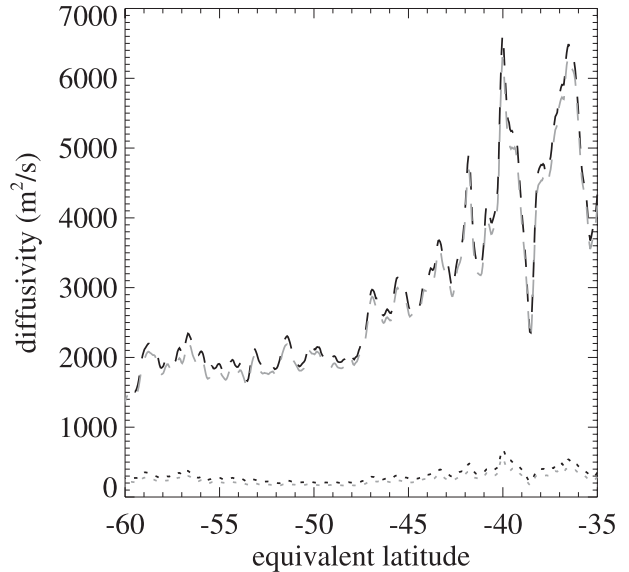


FIG. A1. Latitudinal dependency of surface eddy diffusivity inferred from the tracer analysis with K_λ (dashed line) and K_{Nak} (dotted line), for a relaxation time scale of $\lambda^{-1} = 12$ days. Results are for $k = 50 \text{ m}^2 \text{ s}^{-1}$ (black line) and $k = 100 \text{ m}^2 \text{ s}^{-1}$ (gray line).

the history of the flow (weighted toward the recent past, defined by some “memory time”). The memory time will be shorter when k is larger. Temporary changes in the eddy diffusivity of the flow will be fully represented by K_{eff} only if they persist for longer than the memory time. We believe that the memory time implied by a numerical diffusivity of $k = 50 \text{ m}^2 \text{ s}^{-1}$ is sufficiently small to allow K_{eff} to resolve variations in the mixing ability over time scales of about a month or so (Shuckburgh et al. 2009a).

REFERENCES

Abraham, E., 1998: The generation of plankton patchiness by plankton stirring. *Nature*, **391**, 577–580.
 —, and M. M. Bowen, 2002: Chaotic stirring by a mesoscale surface-ocean flow. *Chaos*, **12**, 373–381.
 Barsugli, J. J., and D. S. Battisti, 1998: The basic effects of atmosphere–ocean thermal coupling on midlatitude variability. *J. Atmos. Sci.*, **55**, 477–493.
 Bourras, D., G. Reverdin, H. Giordani, and G. Caniaux, 2004: Response of the atmospheric boundary layer to a mesoscale oceanic eddy in the northeast Atlantic. *J. Geophys. Res.*, **109**, D18114, doi:10.1029/2004JD004799.
 Bracco, A., S. Clayton, and C. Pasquero, 2009: Horizontal advection, diffusion, and plankton spectra at the sea surface. *J. Geophys. Res.*, **114**, C02001, doi:10.1029/2007JC004671.
 Bretherton, F. P., 1982: Ocean climate modelling. *Prog. Oceanogr.*, **11**, 93–129.
 Frankignoul, C., 1985: Sea surface temperature anomalies, planetary waves and air-sea feedback in the middle latitudes. *Rev. Geophys.*, **23**, 357–390.

- , and E. Kestenare, 2002: The surface heat flux feedback. Part 1: Estimates from observations in the Atlantic and the North Pacific. *Climate Dyn.*, **19**, 633–647.
- , A. Czaja, and B. L'Héveder, 1998: Air–sea feedback in the North Atlantic and surface boundary conditions for ocean models. *J. Climate*, **11**, 2310–2324.
- Greatbatch, R. J., X. Zhai, C. Eden, and D. Olbers, 2007: The possible role in the ocean heat budget of eddy-induced mixing due to air–sea interaction. *Geophys. Res. Lett.*, **34**, L07604, doi:10.1029/2007GL029533.
- Haney, R., 1971: Surface thermal boundary condition for ocean circulation models. *J. Phys. Oceanogr.*, **1**, 241–248.
- Hogg, A. M., W. K. Dewar, P. Berloff, S. Kravtsov, and D. K. Hutchinson, 2009: The effects of mesoscale ocean–atmosphere coupling on the large-scale ocean circulation. *J. Climate*, **22**, 4066–4082.
- Iudicone, D., G. Madec, B. Blanke, and S. Speich, 2008: The role of Southern Ocean surface forcings and mixing in the global conveyor. *J. Phys. Oceanogr.*, **38**, 1377–1400.
- Jin, X., C. Dong, J. Kurian, and J. C. McWilliams, 2009: SST–wind interaction in coastal upwelling: Oceanic simulation with empirical coupling. *J. Phys. Oceanogr.*, **39**, 2957–2970.
- Kalnay, and Coauthors, 1996: The NCEP/NCAR 40-Year Reanalysis Project. *Bull. Amer. Meteor. Soc.*, **77**, 437–471.
- Kramer, P., and S. Keating, 2009: Homogenization theory for a replenishing passive scalar field. *Chin. Ann. Math.*, **30**, 631–644.
- Large, W., and S. Yeager, 2004: Diurnal to decadal global forcing for ocean and sea-ice models: The data sets and flux climatologies. NCAR Tech. Note NCAR/TN-460+STR, 105 pp.
- Levitus, S., and T. Boyer, 1994: *Temperature*. Vol. 4, *World Ocean Atlas 1994*, NOAA Atlas NESDIS 4, 117 pp.
- Lévy, M., 2003: Mesoscale variability of phytoplankton and of new production: Impact of the large-scale nutrient distribution. *J. Geophys. Res.*, **108**, 3358, doi:10.1029/2002JC001577.
- Mahadevan, A., and D. Archer, 2000: Modelling the impact of fronts and mesoscale circulation on the nutrient supply and biogeochemistry of the upper ocean. *J. Geophys. Res.*, **105**, 1209–1225.
- Marshall, J., and G. Shutts, 1981: A note on rotational and divergent eddy fluxes. *J. Phys. Oceanogr.*, **11**, 1677–1680.
- , A. Adcroft, C. Hill, L. Perelman, and C. Heisey, 1997a: A finite-volume, incompressible Navier Stokes model for studies of the ocean on parallel computers. *J. Geophys. Res.*, **102** (C3), 5753–5766.
- , C. Hill, L. Perelman, and A. Adcroft, 1997b: Hydrostatic, quasi-hydrostatic, and nonhydrostatic ocean modeling. *J. Geophys. Res.*, **102** (C3), 5733–5752.
- , H. Jones, R. Karsten, and R. Wardle, 2002: Can eddies set ocean stratification? *J. Phys. Oceanogr.*, **32**, 26–38.
- , E. Shuckburgh, H. Jones, and C. Hill, 2006: Estimates and implications of surface eddy diffusivity in the Southern Ocean derived from tracer transport. *J. Phys. Oceanogr.*, **36**, 1806–1821.
- Nakamura, N., 1996: Two-dimensional mixing, edge formation, and permeability diagnosed in area coordinates. *J. Atmos. Sci.*, **53**, 1524–1537.
- Park, S., C. Deser, and M. Alexander, 2005: Estimation of the surface heat flux response to sea surface temperature anomalies over the global oceans. *J. Climate*, **18**, 4582–4599.
- Pasquero, C., 2005: Differential eddy diffusion of biogeochemical tracers. *Geophys. Res. Lett.*, **32**, L17603, doi:10.1029/2005GL023662.
- Plumb, R. A., 1979: Eddy fluxes of conserved quantities by small-amplitude waves. *J. Atmos. Sci.*, **36**, 1699–1704.
- Radko, T., and J. Marshall, 2004: Eddy-induced diapycnal fluxes and their role in the maintenance of the thermocline. *J. Phys. Oceanogr.*, **34**, 372–383.
- Resplandy, L., M. Lévy, F. d'Ovidio, and L. Merlivat, 2009: Impact of submesoscale variability in estimating the air–sea CO₂ exchange: Results from a model study of the POMME experiment. *Global Biogeochem. Cycles*, **23**, GB1017, doi:10.1029/2008GB003239.
- Richardson, P. L., 1993: A census of eddies observed in North Atlantic SOFAR float data. *Prog. Oceanogr.*, **31**, 1–50.
- Shuckburgh, E., and P. Haynes, 2003: Diagnosing transport and mixing using a tracer-based coordinate system. *Phys. Fluids*, **15**, 3342–3357.
- , W. Norton, A. Iwi, and P. Haynes, 2001: Influence of the quasi-biennial oscillation on isentropic transport and mixing in the tropics and subtropics. *J. Geophys. Res.*, **106**, 14 327–14 337.
- , H. Jones, J. Marshall, and C. Hill, 2009a: Robustness of effective diffusivity diagnostic in oceanic flows. *J. Phys. Oceanogr.*, **39**, 1993–2009.
- , —, —, and —, 2009b: Understanding the regional variability of eddy diffusivity in the Pacific sector of the Southern Ocean. *J. Phys. Oceanogr.*, **39**, 2011–2023.
- Spall, M., 2007: Effect of sea surface temperature–wind stress coupling on baroclinic instability in the ocean. *J. Phys. Oceanogr.*, **37**, 1092–1097.
- Tandon, A., and C. Garrett, 1996: On a recent parameterization of mesoscale eddies. *J. Phys. Oceanogr.*, **26**, 406–411.
- Veneziani, M., A. Griffa, A. M. Reynolds, and A. J. Mariano, 2004: Oceanic turbulence and stochastic models from subsurface Lagrangian data for the northwest Atlantic Ocean. *J. Phys. Oceanogr.*, **34**, 1884–1906.
- Waugh, D., E. Abraham, and M. Bowen, 2006: Spatial variations of stirring in the surface ocean: A case study of the Tasman Sea. *J. Phys. Oceanogr.*, **36**, 526–542.
- Zhai, X., and R. J. Greatbatch, 2006a: Inferring the eddy-induced diffusivity for heat in the surface mixed layer using satellite data. *Geophys. Res. Lett.*, **33**, L24607, doi:10.1029/2006GL027875.
- , and —, 2006b: Surface eddy diffusivity for heat in a model of the northwest Atlantic Ocean. *Geophys. Res. Lett.*, **33**, L24611, doi:10.1029/2006GL028712.